Chapter 3

Modelling

In this chapter, a non-linear mathematical model of a multirotor with a suspended payload will be derived. This model will be used to simulate the multirotor-payload system in subsequent chapters. The model will be based on the real quadrotor named *Honeybee*, which was built by [6] and will be described further in Chapter 6.

The chapter starts by defining the coordinate frames and rotation representations used in this work ~~model~~. A Six-Degrees-of-Freedom (6DOF) model of the quadrotor vehicle will then be derived and the different forces and moments acting on this vehicle will be described. A model of the suspended payload attached to the quadrotor will also be derived. Finally, the mathematical models will be verified against practical flight data from *Honeybee*.

3.1. Coordinate frames

A quadrotor with a standard X-configuration is considered in this work. Figure 3.1 shows a quadrotor schematic and two coordinate frames that will be used to describe this system.

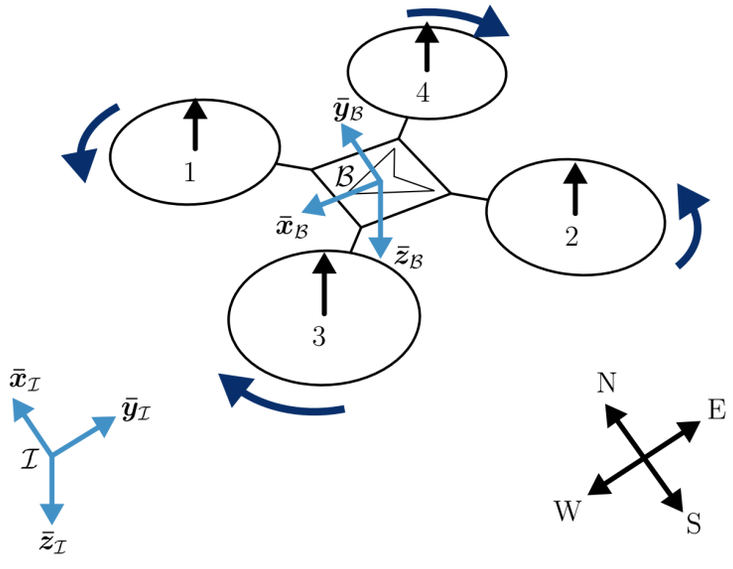

Figure 3.1: Inertial and body coordinate frames of a quadrotor from [2]

The inertial frame is denoted by $\mathcal{I} = \{\bar{\boldsymbol{x}}_\mathcal{I}, \bar{\boldsymbol{y}}_\mathcal{I}, \bar{\boldsymbol{z}}_\mathcal{I}\}$ and describes a North-East-Down (NED) axis system. The x, y, and z axis, align with the North, East, and Down inertial directions respectively. The inertial frame assumes a flat, non-rotating earth since the quadrotor will travel small distances in comparison to the curvature of the earth. The origin of this frame is fixed at the takeoff location of the multirotor.

The body frame is denote by $\mathcal{B} = \{\bar{\boldsymbol{x}}_\mathcal{B}, \bar{\boldsymbol{y}}_\mathcal{B}, \bar{\boldsymbol{z}}_\mathcal{B}\}$ and is fixed to the quadrotor body. The origin of this frame is at the Centre-of-Mass (CoM) of the vehicle and the x, y, and z axes, align with the forwards, rightwards, and downwards directions of the quadrotor body respectively. The body frame is defined by a translation and rotation relative to the inertial frame. The mathematical representation of rotations will be discussed in the section below.

3.2. Rotations

The rotation of the body frame relative to the inertial frame is referred to as the attitude of the multirotor. The attitude ~~will be~~ is defined in terms of Euler angles or quaternions in this work, which ~~will be~~ is described below.

THIS IS WHAT I MEAN WITH OVERUSING THE FUTURE TENSE

3.2.1. Euler angles

Euler angles are a popular way of describing a Three Dimensional (3D) rotation as a sequence of three consecutive elementary rotations [7]. For aircraft applications, the ZYX-sequence is common [7] and ~~will be~~ is used in this work. The order of rotations are:

1. Rotate the body frame about the z-axis by the yaw angle, Ψ.
2. Rotate the resulting frame about the new y-axis by the pitch angle, Θ.
3. Rotate the resulting frame about the new x-axis by the roll angle, Φ.

Figure 3.2 gives a simple illustration of the Euler-ZYX angles. Note that Θ and Φ are each illustrated here as a pure pitch and roll angle from the inertial frame, without a prior Euler rotation.

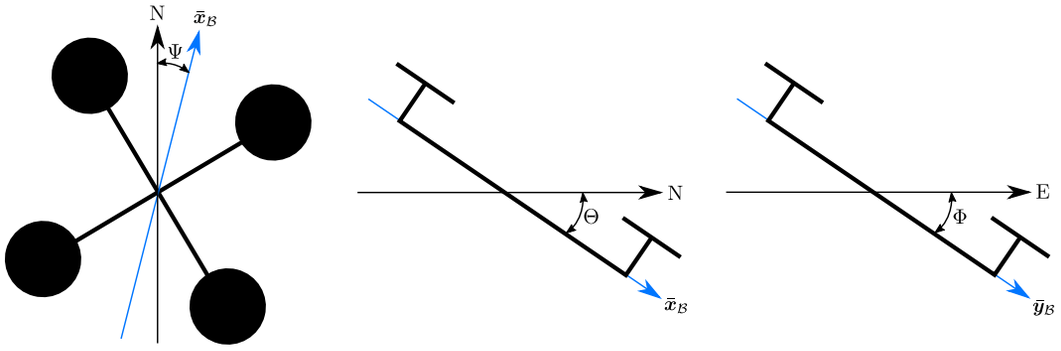

Figure 3.2: Illustration of Euler angles from [3]

3.2.2. Quaternions

A quaternion provides a way of representing a rotation with four parameters. An advantage of quaternions is that it does not produce singularities like Euler angles do [7]. A quaternion defines a rotation with a single rotation about a fixed axis, which is parametrized by a rotation angle, α, and a unit vector, $\mathbf{r}$. A unit quaternion is therefore defined as,

$$\boldsymbol{q} = [q_0 \quad q_1 \quad q_2 \quad q_3]^T = \begin{bmatrix} q_0 \\ \boldsymbol{q}_v \end{bmatrix} = \begin{bmatrix} \cos(\frac{\alpha}{2}) \\ \mathbf{r}\sin(\frac{\alpha}{2}) \end{bmatrix}, \tag{3.1}$$

where q_0 is the magnitude component and $\boldsymbol{q}_v$ is the vector component of the quaternion.

A Euler-ZYX angle representation, $[\Theta \quad \Phi \quad \Psi]$, can be converted to a quaternion with the equation [7],

$$\boldsymbol{q}(\Theta,\Phi,\Psi) = \begin{bmatrix} \cos\frac{\Phi}{2}\cos\frac{\Theta}{2}\cos\frac{\Psi}{2} & + & \sin\frac{\Phi}{2}\sin\frac{\Theta}{2}\sin\frac{\Psi}{2} \\ -\cos\frac{\Phi}{2}\sin\frac{\Theta}{2}\sin\frac{\Psi}{2} & + & \cos\frac{\Theta}{2}\cos\frac{\Psi}{2}\sin\frac{\Phi}{2} \\ \cos\frac{\Phi}{2}\cos\frac{\Psi}{2}\sin\frac{\Theta}{2} & + & \sin\frac{\Phi}{2}\cos\frac{\Psi}{2}\sin\frac{\Psi}{2} \\ \cos\frac{\Phi}{2}\cos\frac{\Theta}{2}\sin\frac{\Psi}{2} & - & \sin\frac{\Phi}{2}\cos\frac{\Psi}{2}\sin\frac{\Theta}{2} \end{bmatrix}. \tag{3.2}$$

The inverse of an quaternion is defined as,

$$\boldsymbol{q}^{-1} = \frac{\begin{bmatrix} q_0 \\ -\boldsymbol{q}_v \end{bmatrix}}{\sqrt{{q_0}^2 + {q_1}^2 + {q_2}^2 + {q_3}^2}}. \tag{3.3}$$

Furthermore, the multiplication of two quaternions, $\boldsymbol{q}$ and $\boldsymbol{q}'$, is given by [7]:

$$\boldsymbol{q} \cdot \boldsymbol{q}' = Q(\boldsymbol{q})\boldsymbol{q}', \tag{3.4}$$

where

$$Q(\boldsymbol{q}) = \begin{bmatrix} q_0 & -q_1 & -q_2 & -q_3 \\ q_1 & q_0 & -q_3 & q_2 \\ q_2 & q_3 & q_0 & -q_1 \\ q_3 & -q_2 & q_1 & q_0 \end{bmatrix}. \tag{3.5}$$

These equations ~~will~~ ~~be~~ is applied in subsequent chapters.

3.3. Quadrotor model

The quadrotor is modelled as a rigid body with six degrees of freedom. This includes three translations and three rotational degrees of freedom. This modelling process is well described by [2] and [3], and the same general procedure is followed ~~in this work.~~

The system parameters describing the physical properties of the quadrotor is listed in Table 3.1. These parameters ~~will be~~ are used in subsequent sections to derive a model of the quadrotor.

Table 3.1: System parameters of the quadrotor model.

Symbol	Description
m_Q	Mass of multirotor
I_{xx}	Mass moment of inertia about $\bar{\boldsymbol{x}}_{\mathcal{B}}$
I_{yy}	Mass moment of inertia about $\bar{\boldsymbol{y}}_{\mathcal{B}}$
I_{zz}	Mass moment of inertia about $\bar{\boldsymbol{z}}_{\mathcal{B}}$
d	Distance from CoM to each motor
R_N	Virtual yaw moment arm
τ	Motor-propeller pair time constant
C_{Q_X}	Aerodynamic drag coefficient in $\bar{\boldsymbol{x}}_{\mathcal{B}}$ direction
C_{Q_Y}	Aerodynamic drag coefficient in $\bar{\boldsymbol{x}}_{\mathcal{B}}$ direction
C_{Q_Z}	Aerodynamic drag coefficient in $\bar{\boldsymbol{x}}_{\mathcal{B}}$ direction

The inertia tensor of the quadrotor is defined as,

$$\boldsymbol{I_Q} = \begin{bmatrix} I_{xx} & I_{xy} & I_{xz} \\ I_{yx} & I_{yy} & I_{yz} \\ I_{zx} & I_{zy} & I_{zz} \end{bmatrix} \approx \begin{bmatrix} I_{xx} & 0 & 0 \\ 0 & I_{yy} & 0 \\ 0 & 0 & I_{zz} \end{bmatrix}. \tag{3.6}$$

The quadrotor is assumed to be symmetrical about the XZ- and YZ-plane, therefore the inertia tensor can be approximated as a diagonal matrix, as shown in Equation 3.6.

The linear velocity and angular velocity of the quadrotor ~~with respect to~~ within the body frame is denoted by,

$$\boldsymbol{V_B} = \begin{bmatrix} V_{B_X} & V_{B_Y} & V_{B_Z} \end{bmatrix}^T, \text{ and} \tag{3.7}$$

$$\boldsymbol{\Omega_B} = \begin{bmatrix} \Omega_{B_X} & \Omega_{B_Y} & \Omega_{B_Z} \end{bmatrix}^T. \tag{3.8}$$

Furthermore, the sum of forces and sum of moments acting on the quadrotor in the body frame are denotes by,

$$\boldsymbol{F_B} = \begin{bmatrix} F_{B_X} & F_{B_Y} & F_{B_Z} \end{bmatrix}^T, \text{ and} \tag{3.9}$$

$$\boldsymbol{M_B} = \begin{bmatrix} M_{B_X} & M_{B_Y} & M_{B_Z} \end{bmatrix}^T. \tag{3.10}$$

As described by [2], these equations can be used with Newton's second law to derive the rigid body equations of motion as,

$$\boldsymbol{F_B} = m_Q \dot{\boldsymbol{V}}_{\boldsymbol{B}} + \boldsymbol{\Omega_B} \times m_Q \boldsymbol{V_B}, \tag{3.11}$$

$$\boldsymbol{M_B} = \boldsymbol{I_Q} \dot{\boldsymbol{\Omega}}_{\boldsymbol{B}} + \boldsymbol{\Omega_B} \times \boldsymbol{I_Q} \boldsymbol{V_B}, \tag{3.12}$$

This provides a set of Ordinary Differential Equations (ODEs) which fully describe the quadrotor motion in 6DOF, given the forces and moments acting on the vehicle. With the equation derived by [8], the attitude of the quadrotor can be obtained as a quaternion from the body angular rates using,

$$\begin{bmatrix} \dot{q}_0 \\ \dot{q}_1 \\ \dot{q}_2 \\ \dot{q}_3 \end{bmatrix} = \frac{1}{2} \begin{bmatrix} q_0 & -q_1 & -q_2 & -q_3 \\ q_1 & q_0 & -q_3 & q_2 \\ q_2 & q_3 & q_0 & -q_1 \\ q_3 & -q_2 & q_1 & q_0 \end{bmatrix} \begin{bmatrix} 0 \\ \Omega_{B_X} \\ \Omega_{B_Y} \\ \Omega_{B_Z} \end{bmatrix}. \tag{3.13}$$

The Direct Cosine Matrix (DCM) is also derived by [8] and can be calculated from the attitude quaternion as,

$$\boldsymbol{R}_V = \begin{bmatrix} q_0^2 + q_1^2 + q_2^2 + q_3^2 & 2(q_1 q_2 + q_0 q_3) & 2(q_1 q_3 - q_0 q_2) \\ 2(q_1 q_2 - q_0 q_3) & q_0^2 - q_1^2 + q_2^2 - q_3^2 & 2(q_2 q_3 + q_0 q_1) \\ 2(q_1 q_3 + q_0 q_2) & 2(q_2 q_3 - q_0 q_1) & q_0^2 - q_1^2 - q_2^2 + q_3^2 \end{bmatrix}. \tag{3.14}$$

$\boldsymbol{R}_V$ is the transformation matrix that describes the rotation from the body frame to the inertial frame such that,

$$\boldsymbol{V_I} = \boldsymbol{R}_V^{-1} \boldsymbol{V_B}, \tag{3.15}$$

~~The forces and moments acting on the quadrotor will be described in the next section.~~

DOES NOT CONTRIBUTE ANY ADDITIONAL KNOWLEDGE.

3.4. Forces and moments

Different phenomena apply forces and moments to the quadrotor during flight. The total force and moment acting on the quadrotor in the body frame are given by,

$$\boldsymbol{F}_{\mathcal{B}} = \boldsymbol{F}_{\mathcal{B}}^{T} + \boldsymbol{F}_{\mathcal{B}}^{A} + \boldsymbol{F}_{\mathcal{B}}^{G} + \boldsymbol{F}_{\mathcal{B}}^{P} \text{ and} \tag{3.16}$$

$$\boldsymbol{M}_{\mathcal{B}} = \boldsymbol{M}_{\mathcal{B}}^{T} + \boldsymbol{M}_{\mathcal{B}}^{A} + \boldsymbol{M}_{\mathcal{B}}^{G} + \boldsymbol{M}_{\mathcal{B}}^{P}. \tag{3.17}$$

The phenomena that cause the different forces and moments are denoted by the ~~sub~~scripts, T, A, G, and P, which refer to actuator thrust, aerodynamic drag, gravity, and the payload respectively. These phenomena are also considered and modelled by [2] and [3].

Actuator thrust

A quadrotor has four rotors which each produce a thrust as shown in Figure 3.1. However, the actuators collectively apply a force, $\boldsymbol{F}_{\mathcal{B}}^{T}$, and moment, $\boldsymbol{M}_{\mathcal{B}}^{T}$, to the vehicle. This force and moment can be represented in terms of virtual actuator thrusts as,

$$\boldsymbol{F}_{\mathcal{B}}^{T} = \begin{bmatrix} 0 \\ 0 \\ \delta_T \end{bmatrix} \quad \text{and} \quad \boldsymbol{M}_{\mathcal{B}}^{T} = \begin{bmatrix} d \cdot \delta_A \\ d \cdot \delta_E \\ R_N \cdot \delta_R \end{bmatrix}, \tag{3.18}$$

where d is the distance from each motor to the quadrotor CoM and R_N is the virtual yaw moment arm which is a property of the motor-propeller configuration. The virtual aileron, elevator, and rudder actuator thrusts are denoted by $d\delta_T$, $d\delta_A$, $d\delta_E$, and $d\delta_R$, respectively. These values are calculated with a mixing matrix, such that,

$$\begin{bmatrix} \delta_T \\ \delta_A \\ \delta_E \\ \delta_R \end{bmatrix} = \begin{bmatrix} 1 & 1 & 1 & 1 \\ -\frac{1}{\sqrt{2}} & \frac{1}{\sqrt{2}} & \frac{1}{\sqrt{2}} & -\frac{1}{\sqrt{2}} \\ \frac{1}{\sqrt{2}} & -\frac{1}{\sqrt{2}} & \frac{1}{\sqrt{2}} & -\frac{1}{\sqrt{2}} \\ 1 & 1 & -1 & -1 \end{bmatrix} \begin{bmatrix} T_1 \\ T_2 \\ T_3 \\ T_4 \end{bmatrix}, \tag{3.19}$$

where $\boldsymbol{T} = [T_1 \quad T_2 \quad T_3 \quad T_4]^T$ is a vector of actual thrust forces produced by the four individual rotors. Each motor-propeller pair receives a thrust setpoint and produces a corresponding thrust. This is modelled with a first order differential equation given by,

$$\dot{\boldsymbol{T}} = \frac{\boldsymbol{T}_{sp} - \boldsymbol{T}}{\tau}, \tag{3.20}$$

where $\boldsymbol{T}_{sp}$ is a vector of thrust setpoints corresponding to $\boldsymbol{T}$, and τ is the time constant of the motor-propeller configuration.

Aerodynamics

Multirotors experience aerodynamic forces due to the relative velocity of air over the vehicle. The aerodynamic model is based on work done by [9] and was also applied successfully by [2] and [3]. The model describes the aerodynamic forces as,

$$\boldsymbol{F}_{\mathcal{B}}^{A} = \frac{1}{2}\rho \boldsymbol{V}_{\mathcal{B}_w} |\boldsymbol{V}_{\mathcal{B}_w}| \boldsymbol{C}_Q \tag{3.21}$$

where ρ is the air density, $\boldsymbol{V}_{\mathcal{B}_w}$ is the relative velocity of air over the quadrotor in the body frame, and $\boldsymbol{C}_Q = [C_{Q_X} \quad C_{Q_Y} \quad C_{Q_Z}]^T$ is the drag coefficients and reference areas lumped into a single damping coefficient per axis. The relative velocity, $\boldsymbol{V}_{\mathcal{B}_w}$, is calculated as

$$\boldsymbol{V}_{\mathcal{B}_w} = -\boldsymbol{V}_{\mathcal{B}} + \boldsymbol{R}_V \boldsymbol{V}_w, \tag{3.22}$$

where $\boldsymbol{V}_w$ is the wind velocity in the inertial frame. It is assumed that the moments caused by aerodynamics, such that,

$$\boldsymbol{M}_{\mathcal{B}}^{A} = \begin{bmatrix} 0 \\ 0 \\ 0 \end{bmatrix}. \tag{3.23}$$

Gravity

Gravity applies a vertical force to the quadrotor in the inertial Down axis. The inertial force is transformed into the body frame with the DCM. No moments are applied to the quadrotor due to gravity. Therefore the total force and moment acting on the quadrotor due to gravity is,

$$\boldsymbol{F}_{\mathcal{B}}^{G} = \boldsymbol{R}_V \begin{bmatrix} 0 \\ 0 \\ m_Q g \end{bmatrix} \quad \text{and} \quad \boldsymbol{M}_{\mathcal{B}}^{G} = \begin{bmatrix} 0 \\ 0 \\ 0 \end{bmatrix}. \tag{3.24}$$

Suspended payload

The suspended payload applies a reaction force, $\boldsymbol{F}_{\mathcal{B}}^{P}$, and moment, $\boldsymbol{M}_{\mathcal{B}}^{P}$, to the quadrotor which is dependant on the dynamics of the suspended payload. The payload and cable also experience gravity and aerodynamic forces which influence its motion. These forces and moments will all be considered in the section below.

3.5. Suspended payload model

The dynamical model of the quadrotor is now fully defined, except for the force and moment applied to the vehicle by the payload. The suspended payload can be modelled as a rigid body that is attached to the quadrotor by a rigid link. Hence, the movement of the quadrotor causes the suspended payload to move too. Due to the acceleration

of the payload, the payload applies a reaction force to the quadrotor through the link. The equations of motion of the suspended payload need to be derived to determine these reaction forces and complete the dynamical model of the quadrotor-payload system.

In this section, the payload model and modelling assumptions will firstly be discussed. Thereafter, the payload equations of motions will be derived with Lagrangian mechanics. Finally, the forces acting on the quadrotor due to the payload will be determined.

Figure 3.3 illustrates a quadrotor with a suspended payload, where m_p is the mass of the payload, and l is the length of the suspended cable. The x-axis and y-axis Euler-ZYX angles in the inertial frame are denoted by θ and ϕ respectively. Furthermore, $\boldsymbol{r}_Q = [x_Q \;\; y_Q \;\; z_Q]^T$ defines the position of the quadrotor CoM in the inertial frame. Likewise, $\boldsymbol{r}_p = [x_p \;\; y_p \;\; z_p]^T$ defines the position of the payload in the inertial frame.

3.5.1. Payload assumptions

The following major assumptions are made regarding the payload model:

- The payload is a point-mass.
- The link is massless.
- The link is rigid.
- The link is attached to the CoM of the multirotor.

The payloads used in the practical setup described in Chapter 6, are small relative to the quadrotor and the attachment point is close to the payload CoM. They are attached with a low-friction ~~swivel~~ joint to the suspended cable, therefore the rotation of the payload around the cable axis has a negligible effect on the quadrotor. Therefore modelling the payload as a point-mass appears to be a reasonable approximation.

The cables used in Chapter 6 have a low mass in comparison to the payloads and have a negligible amount of stretch. ~~Furthermore~~, the cable remains straight and rigid during flight due to the tension applied by the payload. Aggressive manoeuvres may cause periods of zero cable tension where the load is in free-fall and the cable is slack [10]. However, such aggressive manoeuvres will not be considered in this work and the assumption of a rigid, massless cable appears reasonable.

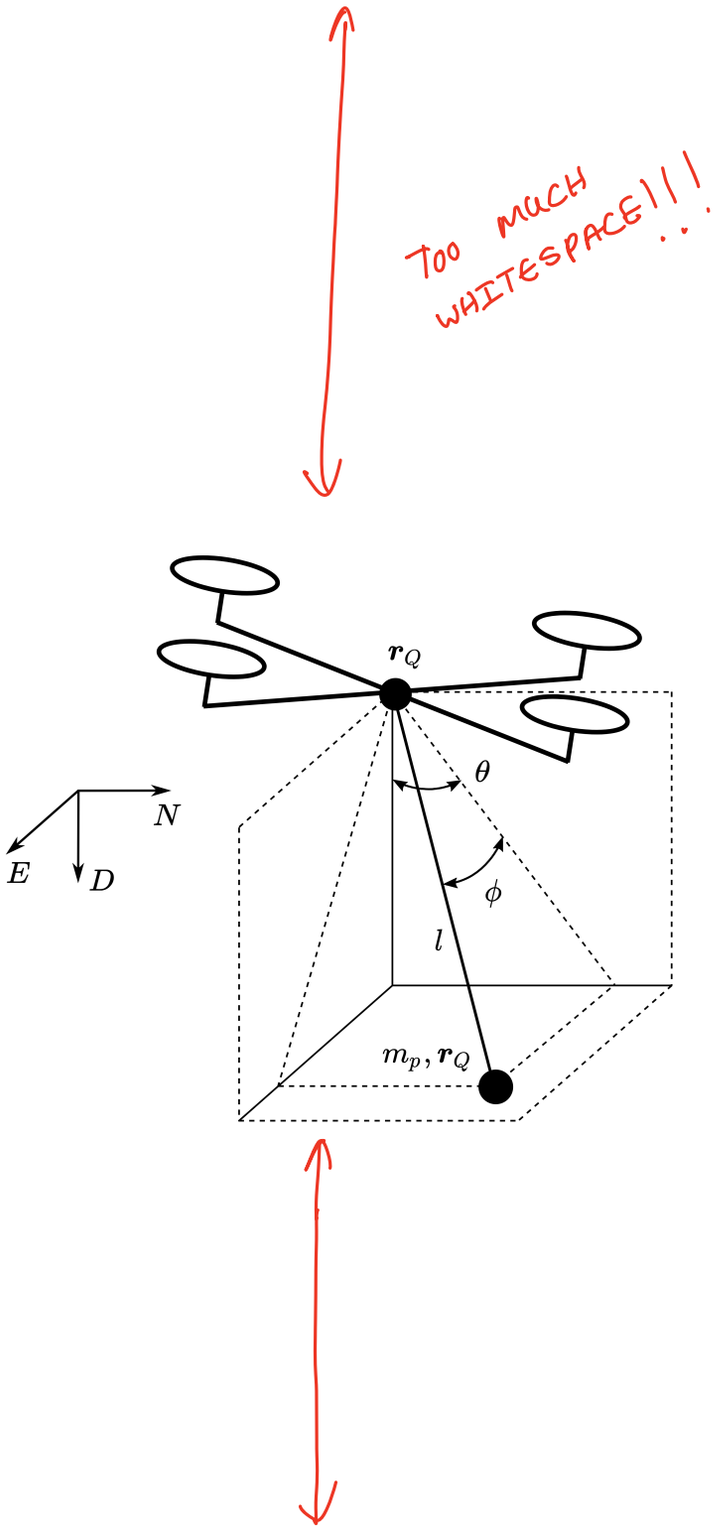

Figure 3.3: Schematic of a quadrotor with suspended payload from [3]

In the practical setup shown in Chapter 6, the cable attachment appears to be near to the CoM of the quadrotor. It is assumed that even if the attachment point is slightly below the actual CoM, this will have a negligible effect on the dynamics and will still be approximated by a CoM attachment. Due to this assumption, the payload cannot apply a moment to the quadrotor, hence the quadrotor attitude dynamics is decoupled from the payload dynamics. Therefore, the quadrotor can be modelled as a point-mass when considering the payload equations of motion.

3.5.2. Lagrangian

Lagrangian mechanics is an energy-based modelling approach that can be used to derive differential equations describing a system [2]. The dynamical equations of the suspended payload system were derived by [3] and the derivation in this work follows parts of that approach. It is important to note that the derivation in this section considers the payload dynamics as a function of the motion of the quadrotor CoM. The derivation starts by defining the payload position as a function of the quadrotor position in the inertial frame as,

$$\boldsymbol{r}_p = \begin{bmatrix} x_p \\ y_p \\ z_p \end{bmatrix} = \begin{bmatrix} x_Q + l\cos(\phi)\sin(\theta) \\ y_Q + \sin(\phi) \\ z_Q + l\cos(\phi)\cos(\theta) \end{bmatrix}, \tag{3.25}$$

where g is the acceleration due to gravity. The vector of generalised coordinates, $\boldsymbol{p}$, of the system can now be defined as,

$$\boldsymbol{p} = \begin{bmatrix} x_p \\ y_p \\ z_p \\ \phi \\ \theta \end{bmatrix}. \tag{3.26}$$

The kinetic energy, $\mathcal{T}_p$, and potential energy, $\mathcal{V}_p$, of the payload can be determined as,

$$\mathcal{T}_p = \frac{1}{2} m_p |\dot{\boldsymbol{r}}_p|^2, \quad \text{and} \tag{3.27}$$

$$\mathcal{V}_p = -m_p g z_p. \tag{3.28}$$

Note that these energy equations describe the system modelled as two point-mass bodies and do not consider the attitude dynamics of the quadrotor as mentioned earlier. The Lagrangian can now be determined as,

$$\mathcal{L} = \mathcal{T}_p - \mathcal{V}_p \tag{3.29}$$

3.5.3. Non-conservative forces

Non-conservative forces and moments refer to effects that add or remove energy from the system. The non-conservative forces and moments acting on the payload include the aerodynamic drag force acting on the payload and the moment caused by the friction of the cable attachment. It is assumed that the cable is thin and short enough that the aerodynamic drag force acting on the cable is negligible.

According to the aerodynamic model presented in Equation 3.21, the aerodynamic drag forces acting on the payload in the inertial frame are defined as,

$$\boldsymbol{F}_p^A = \begin{bmatrix} F_{p_x}^A \\ F_{p_y}^A \\ F_{p_z}^A \end{bmatrix} = \begin{bmatrix} \frac{1}{2}\,\rho\,C_p\,\dot{x_p}^2 \\ \frac{1}{2}\,\rho\,C_p\,\dot{y_p}^2 \\ \frac{1}{2}\,\rho\,C_p\,\dot{z_p}^2 \end{bmatrix}, \tag{3.30}$$

where C_p is the lumped aerodynamic drag coefficient and reference area of the payload. It is assumed that the lumped payload drag coefficients are equal in all three axes, hence it is described by a single coefficient.

Friction at the cable attachment is modelled as linear damping. It is assumed that the coefficient of friction is equal in each axis of rotation. Therefore, the friction moments opposing the θ and ϕ rotations are given by,

$$M_\theta^F = -c\dot{\theta} \tag{3.31}$$

$$M_\phi^F = -c\dot{\phi} \tag{3.32}$$

respectively, where c is the rotational friction coefficient for θ and ϕ rotations. A vector, $\boldsymbol{Q}$, of non-conservative forces and moments corresponding to the system coordinates in $\boldsymbol{p}$ can now be defined as,

$$\boldsymbol{Q} = \begin{bmatrix} -F_{p_x}^A \\ -F_{p_y}^A \\ -F_{p_z}^A \\ M_\theta^F - F_{p_y}^A \cos\phi \\ M_\phi^F - F_{p_x}^A \cos\theta \end{bmatrix}. \tag{3.33}$$

3.5.4. Equations of motion

The set of Euler-Lagrange equations for this system are described by,

$$\frac{d}{dt}\left(\frac{\partial \mathcal{L}}{\partial \dot{p_j}}\right) - \frac{\partial \mathcal{L}}{\partial p_j} = Q_j, \tag{3.34}$$

where p_j is an element in $\boldsymbol{p}$, Q_j is the corresponding element in $\boldsymbol{Q}$, and $j = \{1,\ 2,\ 3,\ 4,\ 5\}$. This set of coupled equations was solved with the Symbolic Maths Toolbox™ [11] in MATLAB to determine the payload equations of motion. This yields a set of ODEs in the form,

$$\ddot{\boldsymbol{p}} = f(\dot{\boldsymbol{p}}, \boldsymbol{p}, \ddot{\boldsymbol{r}}_Q, \dot{\boldsymbol{r}}_Q), \tag{3.35}$$

which describes the motion of the payload as a function of the motion of the quadrotor CoM in the inertial frame.

3.5.5. Payload forces acting on the quadrotor

The reaction force applied to the quadrotor due to the payload can now be determined in the inertial frame as,

$$\boldsymbol{F}_{\mathcal{I}}^{P} = m_Q \ddot{\boldsymbol{r}}_Q, \tag{3.36}$$

from Newton's second law, where $\ddot{\boldsymbol{r}}_Q$ represents the component of the quadrotor acceleration caused by the suspended payload. This force can be represented in the body frame as,

$$\boldsymbol{F}_{\mathcal{B}}^{P} = \boldsymbol{R}_V \boldsymbol{F}_{\mathcal{I}}^{P}. \tag{3.37}$$

~~This completes the quadrotor dynamical model described in Section 3.5~~. The set of ODEs represented by Equation 3.35 provides a coupling between the quadrotor and payload dynamics. The quadrotor-payload system can now be simulated from a given initial condition with an ODE solver in Simulink™. ~~This simulation model will be verified with practical data in the section below.~~

3.6. Model verification

To verify whether the non-linear simulation model derived in previous sections is an accurate representation of the real-world dynamics, the simulation data is verified against practical data. Firstly, a North velocity step response was performed in a practical flight with a quadrotor to verify the quadrotor model without a payload. The practical quadrotor ~~will be~~ is described in Chapter 6. This flight was performed on a day with almost no wind to minimise the effect of wind disturbances in the comparison.

MOVE TO START OF THIS PARAGRAPH

Starting from the same initial condition, ~~the~~ a velocity step setpoint was commanded in ~~a~~ simulation and the resulting simulation data was compared to the practical flight data. This Simulink™ simulation environment ~~will be~~ is discussed in Chapter 5. ~~Note that this~~ and includes the dynamics of the default quadrotor controllers ~~which will be described in Chapter 5~~. ~~Therefore~~ The results ~~in this section~~ compare the combined quadrotor and controller simulation model to the practical flight data.

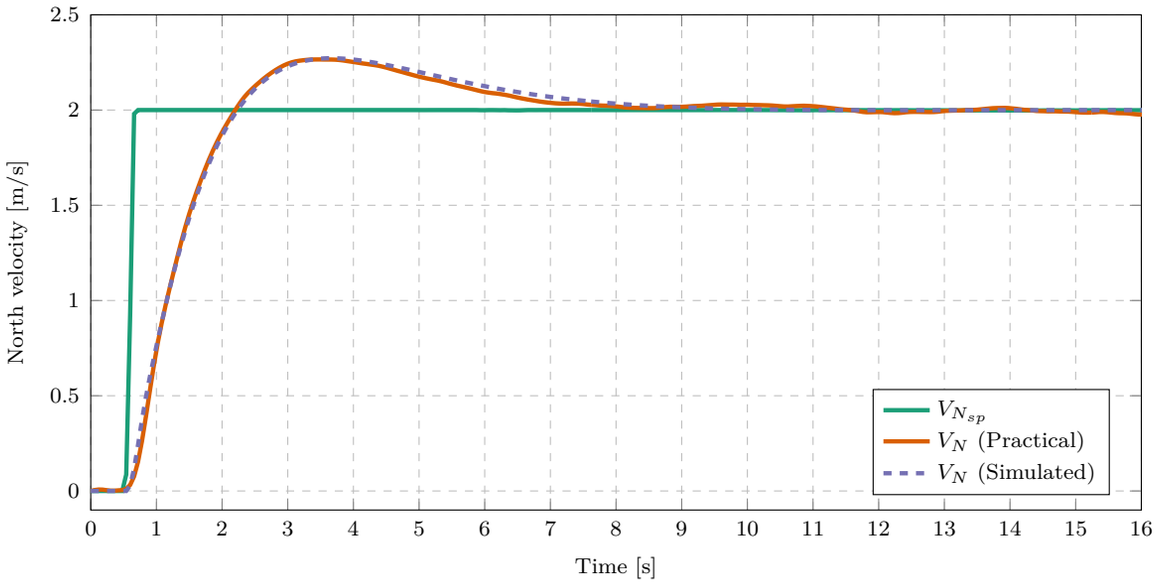

Figure 3.4: Comparison of simulated and practical data from Honeybee

Figure 3.4 shows the velocity step responses of a practical and a simulated flight. From a visual inspection of the plots, it is clear that the velocity responses match well. Note that the practical velocity curve is more irregular and not as smooth as the simulated curve. This may be due to slight wind disturbances or sensor noise, which are not considered in this simulation.

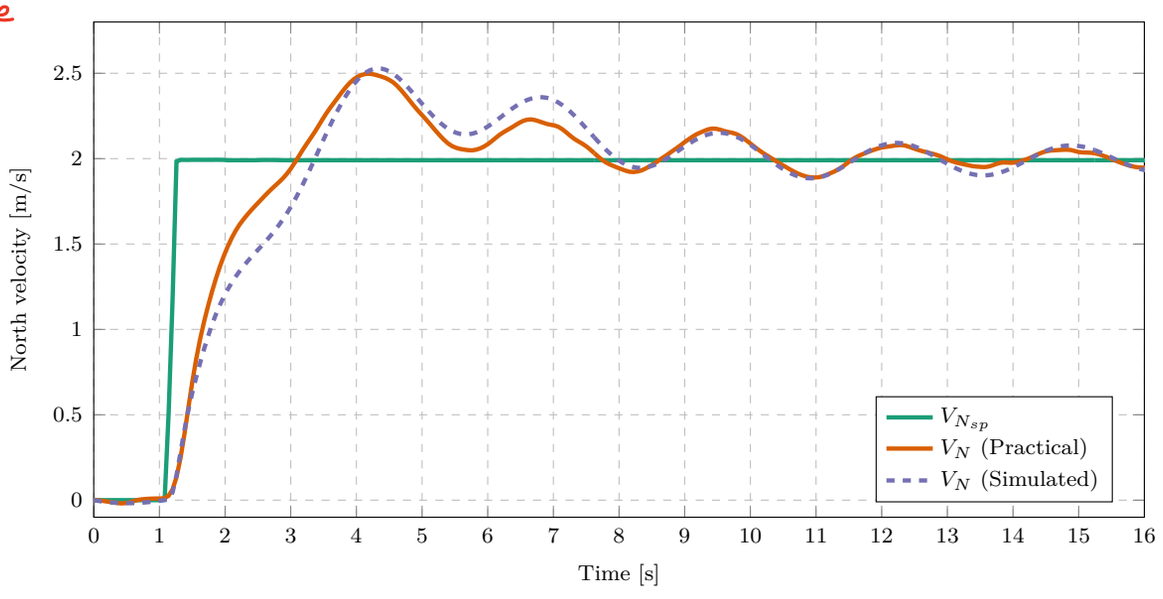

Figure 3.5: Velocity step comparison of simulated and practical data for Honeybee with a suspended payload

The same procedure was followed to verify the quadrotor with a suspended payload model. Figure 3.5 compares the practical and simulated velocity step responses with a suspended payload attached to the vehicle. The shape of the velocity curves also match well in this comparison. However, they do not correlate as well as they do in the no-load experiment.

This may be due to the added complexity of the model. The considered payload model adds modelling assumptions which add to the inaccuracy of the model. The system also considers many state variables that each need to be assigned an accurate initial condition value. Furthermore, the effect of wind disturbances is expected to be greater for the quadrotor-payload system than for the quadrotor without a load.

However, the shape of the practical and simulated velocity curves are still well matched. This seems to be an impressive result for such a complex system with numerous interlinking elements. Both systems provide an overshoot of a similar value. The amplitude and frequency of the velocity oscillations also appear to be very similar.

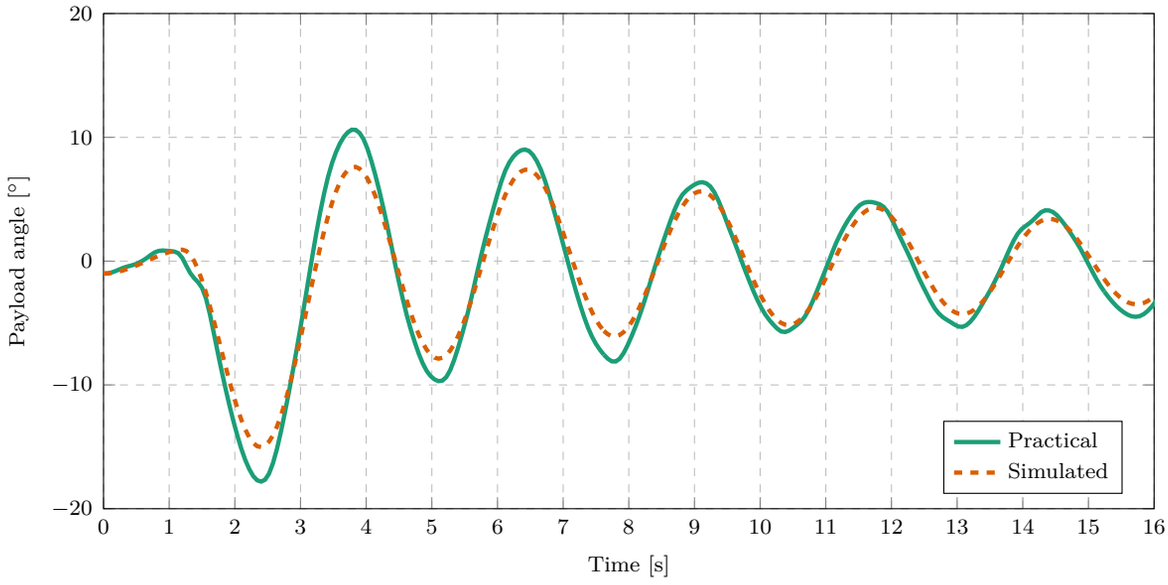

Figure 3.6: Payload angle comparison of simulated and practical data for Honeybee with a suspended payload

Figure 3.6 shows the payload angle for the same flight as Figure 3.5. It is also clear that the payload angle response of the simulated system matches the practical data well. Overall, the results in this section show that the simulation model provides a good representation of the North velocity dynamics of the real quadrotor-payload system. The mathematical model derived in this chapter will therefore be used for further simulations in subsequent chapters.

MAYBE REWORK THIS PARAGRAPH IN A CONCLUSION SECTION. ALL OTHER CHAPTERS HAVE A SEPERATE CONCCLUSION SECTION.